Observation of Electric Hysteresis, Polarization Oscillation, and Pyroelectricity in Nonferroelectric *p-n* Heterojunctions

Yucheng Jiang,[1,2,*,†] Xinglong Ma,[1,3,†] Lin Wang,[3,†] Jinlei Zhang,[1,†] Zhichao Wang,[1] Run Zhao,[1] Guozhen Liu,[1] Yang Li,[1] Cheng Zhang,[1] Chunlan Ma,[1] Yaping Qi,[4,5] Lin Wu,[6,7] and Ju Gao[1,8]

[1]*Jiangsu Key Laboratory of Micro and Nano Heat Fluid Flow Technology and Energy Application, School of Physical Science and Technology, Suzhou University of Science and Technology, Suzhou 215009, China*
[2]*School of Physics, Nanjing University, Nanjing 210093, China*
[3]*School of Materials Science and Engineering, Shanghai University, Shanghai 200444, China*
[4]*Macau Institute of Systems Engineering, Macau University of Science and Technology, Macau 999078, China*
[5]*Advanced Institute for Materials Research, Tohoku University, Sendai 980-8577, Japan*
[6]*Science, Mathematics and Technology, Singapore University of Technology and Design, 8 Somapah Road, Singapore 487372, Singapore*
[7]*Institute of High Performance Computing, Agency for Science, Technology, and Research 1 Fusionopolis Way, #16-16 Connexis, Singapore 138632, Singapore*
[8]*School for Optoelectronic Engineering, Zaozhuang University, Shandong 277160, China*

(Received 12 July 2022; accepted 31 March 2023; published 9 May 2023)

The switchable electric polarization is usually achieved in ferroelectric materials with noncentrosymmetric structures, which opens exciting opportunities for information storage and neuromorphic computing. In another polar system of *p-n* junction, there exists the electric polarization at the interface due to the Fermi level misalignment. However, the resultant built-in electric field is unavailable to manipulate, thus attracting less attention for memory devices. Here, we report the interfacial polarization hysteresis (IPH) in the vertical sidewall van der Waals heterojunctions of black phosphorus and quasi-two-dimensional electron gas on $SrTiO_3$. A nonvolatile switching of electric polarization can be achieved by reconstructing the space charge region (SCR) with long-lifetime nonequilibrium carriers. The resulting electric-field controllable IPH is experimentally verified by electric hysteresis, polarization oscillation, and pyroelectric effect. Further studies confirm the transition temperature of 340 K, beyond which the IPH vanishes. The second transition is revealed with the temperature dropping below 230 K, corresponding to the sharp improvement of IPH and the freezing of SCR reconstruction. This work offers new possibilities for exploring the memory phenomena in nonferroelectric *p-n* heterojunctions.

DOI: 10.1103/PhysRevLett.130.196801

Interfaces in *p-n* heterostructures give rise to many extraordinary physical properties, such as rectification, photovoltaic effect, electroluminescence, etc. [1–5]. Usually, a space charge region (SCR) is induced at the interface due to the complete depletion of major carriers [6]. Residual space charges enable the formation of built-in electric field to prevent a further recombination of electrons and holes [6]. The naturally formed SCR is a suitable platform to study nonequilibrium carriers (NECs), eliminating the interference of intrinsic carriers [7,8]. For example, a usual strategy is to inject photons into the SCR to create the photocarriers as a type of NECs [9,10]. In this case, the built-in barrier is temporarily controlled through the generation and recombination of photocarriers, thus causing several intriguing photoelectric properties [11,12]. An interface of *p-n* junction is regarded as a polar system. A piezoelectric effect can be induced through the interfacial electric polarization [13,14]. However, in most cases, such an interfacial polarization can be changed only by the current physical stimulation but not by its history. This volatile nature limits the possible application of *p-n* heterostructures for memory.

The nonvolatile switching of electric polarization has been widely reported in ferroelectric materials, originating from the ordered arrangement of electric dipoles [15–22]. Ferroelectrics must show electric hysteresis and pyroelectricity, reflecting the nonvolatile change of electric polarization [23–25]. The noncentrosymmetric structure is a crucial premise to achieve the ferroelectricity [26]. For this goal, many methods are employed to break the lattice symmetry of centrosymmetric materials, such as lattice twist, interlayer sliding, strain, and doping [27–33]. Compared with the bulk polarization in ferroelectrics, the interface polarization in heterostructures depends on the distribution of space charges instead of electric dipoles. To achieve the nonvolatile switching of built-in potential, a reasonable strategy is to fill the SCR with long-lifetime NECs through a bias voltage. The switchable interface polarization may emerge due to the reconstruction of the SCR.

 © 2023 American Physical Society

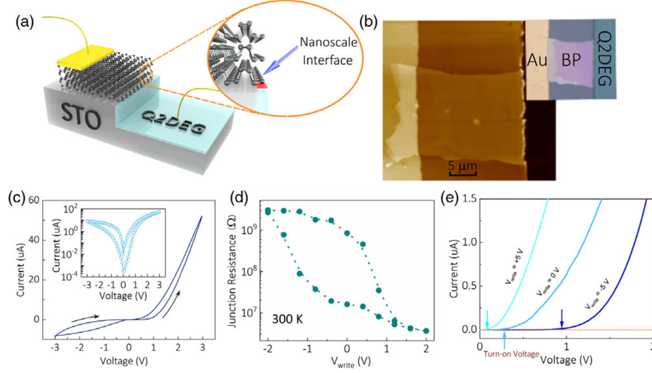

FIG. 1. (a) Structural schematic of BP-Q2DEG heterostructure. (b) AFM image showing the surface morphology of the heterojunction. Inset: photograph of the heterojunction. (c) *I-V* loop measured in the bias range of −3–3 V at 300 K. Inset: semilog *I-V* loop. The arrows reveal the direction of the voltage sweeps. (d) Junction resistance as a function of V_{write} with $V_{read} = 0.2$ V, where V_{write} is a pulsed voltage to drive the device with the pulse width of 1 s. Wait time between V_{write} and V_{read} is 30 s. (e) *I-V* curves in the bias range of 0–2 V after V_{write} pulses of 0, −5, and +5 V. The arrows mark the turn-on voltages.

In this Letter, we report the interfacial polarization hysteresis (IPH) in a vertical sidewall van der Waals (vdW) heterojunction of black phosphorus (BP) and quasi-two-dimensional electron gas (Q2DEG) on $SrTiO_3$ (STO). A nonvolatile switching of electric polarization is experimentally verified by electric hysteresis, polarization oscillation, and pyroelectricity. A transition is observed at 340 K, where the IPH vanishes. The theoretical model is proposed to explain the observed effects based on long-lifetime NECs. This work enriches the functionalities of heterostructure interfaces and extends the applications of *p-n* heterostructures to information recording and electronic storage.

The BP-Q2DEG heterostructures are fabricated using an Ar^+-ion bombardment assistant method reported by our recent works (see Sec. 1 and Fig. S1 in the Supplemental Material [34]) [9,35,36]. Figure 1(a) shows a structural schematic of the IPH device on a STO substrate. A vdW contact is formed at the edge of the BP layer and the Q2DEG. Because of the *p*-type conduction of intrinsic BP, a *p-n* junction should be constructed in the interface of BP and the Q2DEG. The excessive Ar^+-ion bombardment is applied to etch a vertical sidewall of Q2DEG on STO during the fabrication, forming a sharp interface in nanoscale. Such a quasi-one-dimensional junction contact can constrain the drift and diffusion processes of free carriers at the interface, thereby reducing the recombination of NECs. This is a structural basis for the ferroelectricitylike effect. For comparison, we fabricated a BP-Q2DEG heterojunction with two-dimensional junction contact [see Fig. S2(a) in the Supplemental Material [34]]. No hysteresis behavior can be observed in this device. Their difference demonstrates the important role of the quasi-one-dimensional interface in the charge trapping [see Figs. S2(b) and S2(c) in the Supplemental Material [34]]. In Fig. 1(b), the atomic force microscopy (AFM) image and photograph (inset) display the surface morphology of the device with BP thickness of 51 nm and the Ar^+-ion etching depth of 100 nm. Figure 1(c) shows the current-voltage (*I-V*) characteristic investigated in the bias range of −3–3 V at 300 K, demonstrating a rectifying behavior. Hysteresis in the current is observed in the BP-Q2DEG heterostructure [inset in Fig. 1(c)], distinguishing it from normal *p-n* junctions. Along the positive bias voltage, the backward current is greater than the forward current, while the negative bias voltage gives rise to an opposite effect. Furthermore, a large pulsed write voltage (V_{write}) is applied to drive the device for the resistive switching, and a small read voltage (V_{read}) is used to measure the junction resistance. In Fig. 1(d), we observe the hysteresis dependence of junction resistance on V_{write} with an on/off resistive ratio of ∼100. The device exhibits a resistive hysteresis behavior similar to a ferroelectric tunnel junction (FTJ) [37–39]. The FTJ is constructed of a ferroelectric layer sandwiched between two conductors, where the polarization of the ferroelectric layer induces the resistive switching. Because of their similarity, the nonvolatile switching of electric polarization must exist at the BP-Q2DEG interface, showing a FTJ-type resistive switching. This FTJ-like device based on the IPH possesses a good retention in on/off resistance states (see Sec. 2 and Fig. S3 in the Supplemental Material [34]). And the hysteretic resistance curve maintains highly reproducible over 300 circles of voltage sweep, showing good endurance (see Sec. 2 and Fig. S4 in the Supplemental Material [34]). In Fig. 1(e), we compare the *I-V* curves in the bias range of 0–2 V after 0, −5, and +5 V pulsed voltages. The bias voltage causes the nonvolatile change of turn-on voltage. Since the turn-on voltage is attributed to the built-in potential in a *p-n* junction, our observations reflect the nonvolatile dependence of built-in potential on the external electric field, supporting the IPH effect.

As is well known, there is a permanent spontaneous electric polarization at the interface of a *p-n* heterojunction, which is described by the built-in electric field (E_{bi}) [6]. Normally, the built-in potential (V_{bi}) is determined by the carrier densities of *p* and *n* materials and thus independent of any external electric field. However, in the BP-Q2DEG heterostructure, we think that the NECs, injected by an external electric field, cannot recombine instantly after removing the electric field. The remaining NECs will reconstruct the space charge region. So-formed metastable V_{bi} enables the nonvolatile switching through the external electric field, similar to the electric polarization in ferroelectricity. To verify this, few-layer BP and Q2DEG are respectively measured for their photoelectric properties, demonstrating a very long lifetime of NECs (see Sec. 3 and Fig. S5 in the Supplemental Material [34]). In Fig. 2(a),

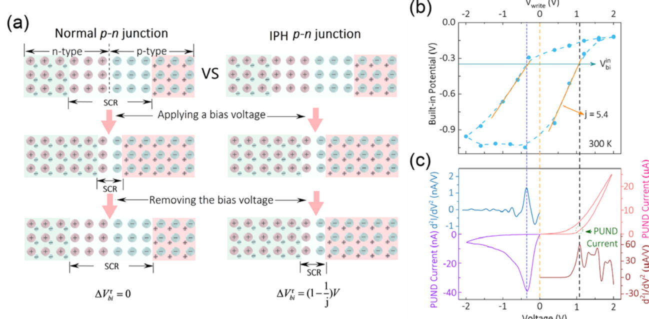

FIG. 2. (a) Schematic showing the dependence of built-in potential on the bias voltage for normal and IPH heterojunctions. (b) V_{bi}-bias hysteresis loop at 300 K, exhibiting the nonvolatile electric polarization. (c) Displacement current detected by a PUND method. Interval time of voltage pulse is 0.2 s. The second derivatives of PUND currents (d^2I/dV^2) are shown in upper left and lower right, to exclude the influence of background current.

the schematic diagram compares normal and IPH p-n junctions. For a normal p-n junction, V_{bi} is changed by the external electric field but recovers to its intrinsic value at zero field. In contrast, the change in V_{bi} is maintained in the absence of external electric field and proportional to the change of electric polarization at the interface. Based on the above understanding, we propose that the change of remanent built-in potential (V_{bi}^r) should satisfy the following formula (see Sec. 4 in the Supplemental Material for the theoretical model [34]),

$$\Delta V_{bi}^r = V_{bi}^r - V_{bi}^{in} = \left(1 - \frac{1}{j}\right)V, \tag{1}$$

where j is a parameter determined by the NEC lifetime ($j \geq 1$), V_{bi}^{in} is the intrinsic built-in potential, and V is the bias voltage. V_{bi}^{in} is an initial state in analogy with zero polarization in ferroelectricity. ΔV_{bi}^r reflects the reconstruction of SCR, which remains after removing the bias voltage. Such a linear relation indicates that a transient application of bias voltage can induce a nonvolatile change of built-in potential, demonstrating a ferroelectricitylike hysteresis behavior, that is, the IPH. The long lifetime of NECs distinguishes IPH junctions from normal junctions (see Fig. S6 in the Supplemental Material [34]). It is noted that the j value depends on both NEC lifetime and temperature. For a normal p-n junction, the lifetime of NECs is extremely short, making j equal to 1. Bias voltage cannot cause the nonvolatile change of built-in potential. To have $j > 1$, it is necessary to prolong the NEC lifetime and lower the temperature. In an IPH junction, the NECs created by the bias voltage will maintain the reconstruction of the SCR even with the field removed.

The change of electric polarization in the IPH effect is realized by SCR reconstruction, differing from the reversal of electric dipoles in the ferroelectricity. A ferroelectric can switch between positive and negative polarizations. In contrast, for an IPH junction, the built-in potential is determined by p- and n-type materials, whose sign cannot be flipped. Its remanent built-in potential tends to decrease or increase by applying a positive or negative bias voltage. However, the different physical processes induce similar polarization switching results, thus leading to similar ferroelectric properties. To verify them, we attempt to investigate hysteresis behavior, positive-up-negative-down (PUND) and pyroelectricity in BP-Q2DEG heterostructures. Figure 2(b) shows the $V_{bi}^r - V_{write}$ hysteresis loop of a BP-Q2DEG heterojunction at 300 K, supporting the nonvolatile dependence of built-in potential on the electric field. Through the slope along the bias voltage, we can calculate the value of j that is about 5.4. Figure 2(c) shows the PUND measurement to detect the displacement current caused by the switching of interface polarization. At negative bias, the PUND current is significantly observed due to the low leakage current, and reaches the peak value at -0.35 V. By contrast, at the positive bias, the background current is so large as to conceal the PUND current. Only a small bulge of current emerges to confirm the existence of PUND current, highlighted by a circle in Fig. 2(b). For ferroelectricity, the PUND current peaks at $\vec{P} = 0$, where electric dipoles have the maximum speed of rotation [40]. Similarly, for the IPH, the PUND peak corresponds to the peak voltage (V_{pk}) to satisfy $\Delta V_{bi} = V_{pk} - V_{bi}^{in} = 0$. Combining the hysteresis loop in Fig. 2(b), it is worth pointing out that the position of the PUND peak along negative bias reflects the intrinsic built-in potential. After the saturated electric polarization at positive bias, the increase of negative voltage will enlarge V_{bi}. With the negative voltage equal to V_{bi}^{in}, all of the NECs, filled by previous positive bias, are completely exhausted. At this point, V_{bi} reaches the maximum rate of change, thus deducing $V_{pk} \approx V_{bi}^{in}$. In order to exclude the influence of background current, we take the second derivative for the measured current [see the insets in Fig. 2(c)]. It is intriguing to observe the interface polarization oscillations in the BP-Q2DEG heterostructure, which originates from two competing physical processes. The SCR width will decrease (or increase) with the positive (or negative) bias applied. On the other hand, it always tends to recover to its intrinsic status. Experimentally, the competition between change and recovery of SCR is reflected by the oscillation curve of the PUND current [see Fig. S7(a) in the Supplemental Material [34]]. Our theoretical model indicates that such a polarization oscillation obeys the Bessel function [see Sec. 5 and Figs. S7 (b) and S7(c) in the Supplemental Material [34]]. The observation of polarization oscillations is important evidence to distinguish the IPH p-n heterojunction from a normal one. In addition, it is worth pointing out that the observed IPH effect cannot be attributed to the bias-induced structural change. Previous works demonstrated that the filament

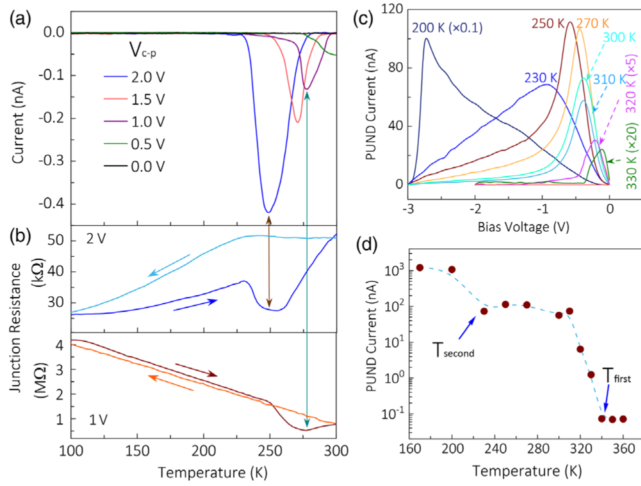

FIG. 3. (a) Pyroelectric responses upon heating from 100 to 300 K after applying different $V_{c\text{-}p}$. The electric poling is performed by cooling the heterojunction to 100 K at the bias range of 0–2 V. (b) Junction resistances as a function of temperature at bias voltages of 1 and 2 V, where the temperature drops to 100 K and then rises to 300 K. (c) PUND responses at different temperatures. (d) Temperature dependence of PUND current, showing the first and second transition temperatures.

channel formation can induce a low resistive state by opening up conductive channels [41,42]. But there is no switching of electric polarization in this case, disagreeing with our experimental results.

The significant pyroelectric currents are observed upon heating from 100 to 300 K in Fig. 3(a), with the heterojunction polarized at various poling voltages ($V_{c\text{-}p}$) upon cooling. The IPH pyroelectricity shows a different mechanism from that of ferroelectricity. For the IPH, after a positive polarization, the SCR is filled by more carriers than its intrinsic state. With the temperature rising over the pyroelectric temperature (T_{py}), the IPH effect disappears and the extra carriers are released to the external circuit, observed as a pyroelectric effect. Another intriguing observation is that the T_{py} of IPH decreases as the $V_{c\text{-}p}$ increases, different from the T_{py} of ferroelectricity that depends only on the ferroelectric phase transition but not the electric polarization degree. This implies that the IPH transition temperatures are different at different depths of SCR (see Sec. 6 and Fig. S8 in the Supplemental Material [34]). Figure 3(b) shows the junction resistance as a function of temperature at bias voltages of 1 and 2 V, where the heterojunction is first cooled to 100 K, and then heated to 300 K. It is noted that the heating curve exhibits a sudden drop in junction resistance precisely at T_{py}, compared to the cooling curve. The current change upon heating cannot be attributed only to the pyroelectric current, since the former is over 4 orders of magnitude larger than the latter. A reasonable explanation is that the sharp shortening of SCR causes the junction resistance to decrease due to the excessive gain of NECs during the pyroelectric process. The experimental results in Figs. 3(a) and 3(b) provide strong evidence to support the conclusion that the IPH originates from the nonvolatile change of local NEC density induced by an external electric field, which rules out the possible mechanism of ion drift (see the detailed analysis in Sec. 7 in the Supplemental Material [34]) [43]. Generally speaking, the IPH shows similar physical phenomena to the ferroelectricity, but there are still specific differences (see Table SI in the Supplemental Material for comparison [34]).

PUND measurements were performed to investigate the temperature dependence of IPH in Fig. 3(c). The PUND current peak shifts to the small bias as the temperature rises, indicating the decrease of $V_{\text{bi}}^{\text{in}}$. Here, we use the PUND current to quantify the IPH. Figure 3(d) shows that the IPH vanishes above the first transition temperature (T_{first}) of 340 K, with the PUND current less than 1 pA. The first transition refers to the emergence of IPH effect. The BP-Q2DEG heterojunction exhibits a potential application as a room-temperature IPH memory device. Another interesting observation is the second transition temperature (T_{second}) of 230 K, where the PUND current increases sharply over 1 order of magnitude. The heterojunction has a larger IPH below 230 K. Moreover, the dependence of IPH on BP thickness is investigated as shown in Fig. S9 in the Supplemental Material [34]. The on/off resistive ratio and T_{first} are enhanced with the increase of BP thickness. With the thickness over 50 nm, the IPH becomes saturated and independent of the BP thickness.

As a IPH device, the BP-Q2DEG heterojunction possesses some new features besides those ferroelectricitylike behaviors. Here, we report the freezing effect of intrinsic SCR accompanied by the second transition. Figure 4(a) shows the junction resistance-temperature (R_j-T) curves at the bias voltage of 1.5 V. The electrical measurements start at 10 K, where the device is insulating. With the electric voltage applied, the device is heated up to 300 K, and then cools back to 10 K. Surprisingly, R_j upon heating is almost 5 orders of magnitude higher than that upon cooling. A giant separation of junction resistances upon heating and cooling occurs within a narrow temperature window of 180–230 K. To understand this phenomenon, we plotted the R_j-T curves upon cooling in different temperature ranges, as shown in Fig. 4(b). It is found that the initial temperature (T_{int}), where to start an R_j-T measurement upon cooling, plays an important role in determining the electronic transport at low temperature. With T_{int} higher than 230 K, the R_j-T curves coincide with each other, indicating that the application of bias voltage at 230–300 K cannot induce a permanent change of low-temperature resistance. The low-temperature resistance tends to increase as T_{int} decreases in the range of 180 to 230 K. With the temperature below 180 K, all junction resistances remain almost constant, no matter what the T_{int} is. Our experimental results demonstrate that an application of bias voltage to the BP-Q2DEG heterojunction at high temperature has a

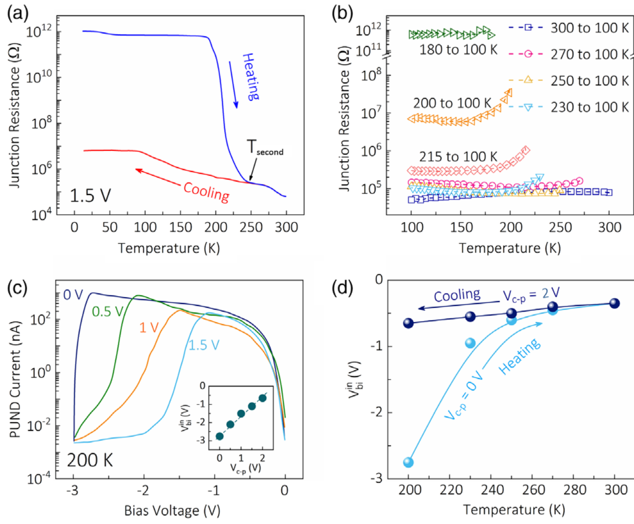

FIG. 4. (a) Junction resistance versus temperature at a bias voltage of 1.5 V. Before the electrical measurement, the BP-Q2DEG heterojunction is cooled down to 10 K at zero bias. Then, the measurement is performed upon heating from 10 to 300 K with a bias voltage applied to obtain the heating curve. The cooling curve is made with the temperature decreasing from 300 to 10 K at the same bias voltage. (b) R_j-T curves upon cooling from different T_{int} to 100 K at a bias voltage of 2 V, where T_{int} is the initial temperature to start the measurement. (c) PUND measurements at 200 K with different $V_{c\text{-}p}$. Inset: the linear relation between $V_{\text{bi}}^{\text{in}}$ and $V_{c\text{-}p}$. (d) Temperature dependence of PUND peak voltage, where the heating curve is measured with zero poling and the cooling curve is obtained at $V_{c\text{-}p} = 2$ V.

permanent effect on the junction resistance at low temperature, which cannot be explained only by the IPH. We think that the freezing of SCR reconstruction occurs when the electric polarization at the interface is maintained below T_{second}. The metastable built-in potential shaped by bias voltage at high temperature becomes an intrinsic state at low temperature. Figure 4(c) shows the PUND currents under the negative voltage at 200 K after various $V_{c\text{-}p}$. Despite the same temperature, the PUND peak voltages are different from each other, greatly determined by $V_{c\text{-}p}$. As we know, the V_{pk} reflects the intrinsic built-in potential. The value of $V_{\text{bi}}^{\text{in}}$ is significantly decreased by $V_{c\text{-}p}$, with the linear relation of $\Delta V_{\text{bi}}^{\text{in}} = V_{c\text{-}p}$. The inset in Fig. 4(c) verifies the linear dependence of $V_{\text{bi}}^{\text{in}}$ on $V_{c\text{-}p}$. The freezing SCR reconstruction can also be investigated by measuring $V_{\text{bi}}^{\text{in}}$ as a function of temperature. In Fig. 4(d), in the absence of $V_{c\text{-}p}$, the PUND peak voltage decreases significantly from −2.8 to −0.34 V upon heating. However, with $V_{c\text{-}p} = 2$ V, the BP-Q2DEG heterojunction shows a slight increase of V_{pk} from −0.34 to −0.75 V upon cooling. The separation of intrinsic built-in potentials upon cooling and heating is just observed near 230 K, which is consistent with the experimental results in Figs. 4(a) and 4(b). One can control the intrinsic built-in potential as desired at low temperature, implying an application for temperature memory. The second transition does not only signify the further improvement of the IPH, but also the freezing effect of SCR reconstruction. It indicates that the NECs injected above T_{second} can transform into equilibrium carriers upon cooling below T_{second}. The emergence of IPH is a necessary prerequisite for the freezing effect. The nonvolatile change of SCR is achieved due to the IPH through the first transition. Then, such a metastable change of SCR can be turned into the intrinsic state through the second transition, with the temperature dropping below T_{second}.

In summary, we have fabricated the BP-Q2DEG vertical sidewall vdW heterostructures through the Ar^+-ion bombardment assistant method. A new physical effect of IPH is found at room temperature, based on the nonvolatile switching of V_{bi} induced by bias voltage. The IPH shows several properties similar to the ferroelectricity, such as electric hysteresis, PUND current, and pyroelectricity. The IPH transition occurs at $T_c = 340$ K. In addition, the second transition is observed with the temperature dropping below 230 K, causing the sharp improvement of IPH and the freezing of SCR reconstruction. Our theoretical model indicates the IPH is attributed to the NECs with a long lifetime. Our work establishes a new platform for switchable electric polarization and expands the scope of ferroelectric materials.

This work was supported by National Natural Science Foundation of China (Grants No. 12274316, No. 12074282, No. 11974304, No. 62004136, No. 22008164), Applied Fundamental Research Foundation of Nantong City, China (No. JC 2021100), the Natural Science Foundation of Jiangsu Province (Grant No. BK20190939), and the Natural Science Foundation of the Jiangsu Higher Education Institutions of China (Grant No. 19KJB150018). Y. Q. acknowledges Macau Science and Technology Development Fund 0031/2021/ITP. L. W. gratefully acknowledges the Start-Up Research Grant from Singapore University of Technology and Design via Grant No. SRG SMT 2021 169, and National Research Foundation Singapore via Grants No. NRF2021-QEP2-02-P03, No. NRF2021-QEP2-03-P09, and No. NRF-CRP26-2021-0004.

*jyc@usts.edu.cn
†These authors contributed equally to this work.

[1] S. Gong, Z. Wang, L. Ye, R. Zhao, G. Liu, J. Zhang, Y. Li, Z. Wu, L. Wang, J. Wang, C. Ma, Y. Jiang, and J. Gao, ACS Appl. Nano Mater. **4**, 10477 (2021).
[2] D. Jariwala, K. Sangwan Vinod, C.-C. Wu, L. Prabhumirashi Pradyumna, L. Geier Michael, J. Marks Tobin, J. Lauhon Lincoln, and C. Hersam Mark, Proc. Natl. Acad. Sci. U.S.A. **110**, 18076 (2013).
[3] N. J. Jeon, J. H. Noh, Y. C. Kim, W. S. Yang, S. Ryu, and S. I. Seok, Nat. Mater. **13**, 897 (2014).

[4] H. Kim, D. Kim Young, T. Wu, Q. Cao, P. Herman Irving, J. Hone, J. Guo, and L. Shepard Kenneth, Sci. Adv. **8**, eabj1742 (2022).

[5] M. Paur, A. J. Molina-Mendoza, R. Bratschitsch, K. Watanabe, T. Taniguchi, and T. Mueller, Nat. Commun. **10**, 1709 (2019).

[6] D. A. Neamen, *Semiconductor Physics and Devices: Basic Principles* (McGraw-hill, New York, 2003).

[7] P. Kloth, K. Kaiser, and M. Wenderoth, Nat. Commun. **7**, 10108 (2016).

[8] V. D. Mihailetchi, J. Wildeman, and P. W. M. Blom, Phys. Rev. Lett. **94**, 126602 (2005).

[9] Y. Jiang, A. He, R. Zhao, Y. Chen, G. Liu, H. Lu, J. Zhang, Q. Zhang, Z. Wang, C. Zhao, M. Long, W. Hu, L. Wang, Y. Qi, J. Gao, Q. Wu, X. Ge, J. Ning, A. T. S. Wee, and C.-W. Qiu, Phys. Rev. Lett. **127**, 217401 (2021).

[10] O. J. Sandberg, S. Dahlstrom, M. Nyman, S. Wilken, D. Scheunemann, and R. Osterbacka, Phys. Rev. Appl. **12**, 034008 (2019).

[11] Q. Bian, F. Ma, S. Chen, Q. Wei, X. Su, I. A. Buyanova, W. M. Chen, C. S. Ponseca, M. Linares, K. J. Karki, A. Yartsev, and O. Inganäs, Nat. Commun. **11**, 617 (2020).

[12] Q. Zhao, A. Hazarika, X. Chen, S. P. Harvey, B. W. Larson, G. R. Teeter, J. Liu, T. Song, C. Xiao, L. Shaw, M. Zhang, G. Li, M. C. Beard, and J. M. Luther, Nat. Commun. **10**, 2842 (2019).

[13] Z. Fan, H. Fan, L. Yang, P. Li, Z. Lu, G. Tian, Z. Huang, Z. Li, J. Yao, Q. Luo, C. Chen, D. Chen, Z. Yan, M. Zeng, X. Lu, X. Gao, and J.-M. Liu, J. Mater. Chem. C **5**, 7317 (2017).

[14] M. M. Yang, Z. D. Luo, Z. Mi, J. Zhao, S. P. E, and M. Alexe, Nature (London) **584**, 377 (2020).

[15] A. Chanthbouala, V. Garcia, R. O. Cherifi, K. Bouzehouane, S. Fusil, X. Moya, S. Xavier, H. Yamada, C. Deranlot, N. D. Mathur, M. Bibes, A. Barthélémy, and J. Grollier, Nat. Mater. **11**, 860 (2012).

[16] D.-W. Fu, H.-L. Cai, Y. Liu, Q. Ye, W. Zhang, Y. Zhang, X.-Y. Chen, G. Giovannetti, M. Capone, and J. Li, Science **339**, 425 (2013).

[17] D. Ji, S. Cai, T. R. Paudel, H. Sun, C. Zhang, L. Han, Y. Wei, Y. Zang, M. Gu, Y. Zhang, W. Gao, H. Huyan, W. Guo, D. Wu, Z. Gu, E. Y. Tsymbal, P. Wang, Y. Nie, and X. Pan, Nature (London) **570**, 87 (2019).

[18] J. Li, C. Ge, J. Du, C. Wang, G. Yang, and K. Jin, Adv. Mater. **32**, 1905764 (2020).

[19] K. M. Ok, E. O. Chi, and P. S. Halasyamani, Chem. Soc. Rev. **35**, 710 (2006).

[20] F. Scott James and A. Paz de Araujo Carlos, Science **246**, 1400 (1989).

[21] R. K. Vasudevan, N. Balke, P. Maksymovych, S. Jesse, and S. V. Kalinin, Appl. Phys. Rev. **4**, 021302 (2017).

[22] A. von Hippel, Rev. Mod. Phys. **22**, 221 (1950).

[23] Z. Fei, W. Zhao, T. A. Palomaki, B. Sun, M. K. Miller, Z. Zhao, J. Yan, X. Xu, and D. H. Cobden, Nature (London) **560**, 336 (2018).

[24] F. Liu, L. You, K. L. Seyler, X. Li, P. Yu, J. Lin, X. Wang, J. Zhou, H. Wang, H. He, S. T. Pantelides, W. Zhou, P. Sharma, X. Xu, P. M. Ajayan, J. Wang, and Z. Liu, Nat. Commun. **7**, 12357 (2016).

[25] R. W. Whatmore, Rep. Prog. Phys. **49**, 1335 (1986).

[26] L. Qi, S. Ruan, and Y.-J. Zeng, Adv. Mater. **33**, 2005098 (2021).

[27] S. Mueller, J. Mueller, A. Singh, S. Riedel, J. Sundqvist, U. Schroeder, and T. Mikolajick, Adv. Funct. Mater. **22**, 2412 (2012).

[28] S. Salmani-Rezaie, K. Ahadi, W. M. Strickland, and S. Stemmer, Phys. Rev. Lett. **125**, 087601 (2020).

[29] M. Vizner Stern, Y. Waschitz, W. Cao, I. Nevo, K. Watanabe, T. Taniguchi, E. Sela, M. Urbakh, O. Hod, and M. Ben Shalom, Science **372**, 1462 (2021).

[30] A. Weston *et al.*, Nat. Nanotechnol. **17**, 390 (2022).

[31] R. Xu, J. Huang, E. S. Barnard, S. S. Hong, P. Singh, E. K. Wong, T. Jansen, V. Harbola, J. Xiao, B. Y. Wang, S. Crossley, D. Lu, S. Liu, and H. Y. Hwang, Nat. Commun. **11**, 3141 (2020).

[32] X. Liu, A. P. Pyatakov, and W. Ren, Phys. Rev. Lett. **125**, 247601 (2020).

[33] Y. Wan, T. Hu, X. Mao, J. Fu, K. Yuan, Y. Song, X. Gan, X. Xu, M. Xue, X. Cheng, C. Huang, J. Yang, L. Dai, H. Zeng, and E. Kan, Phys. Rev. Lett. **128**, 067601 (2022).

[34] See Supplemental Material at http://link.aps.org/supplemental/10.1103/PhysRevLett.130.196801 for experimental processes, retention and endurance, material and structural basis of IPH, theoretical model of IPH, polarization oscillation, mechanism of IPH pyroelectricity and figures.

[35] Y. Chen, A. He, G. Liu, R. Zhao, J. Gao, and Y. Jiang, Appl. Phys. Lett. **115**, 241603 (2019).

[36] Y. Jiang, A. He, K. Luo, J. Zhang, G. Liu, R. Zhao, Z. Qing, W. Zhuo, C. Zhao, L. Wang, Y. Qi, J. Gao, K. P. Loh, A. T. S. Wee, and C.-W. Qiu, Proc. Natl. Acad. Sci. U.S.A. **119**, e2115939119 (2022).

[37] V. Garcia and M. Bibes, Nat. Commun. **5**, 4289 (2014).

[38] H. Lu, A. Lipatov, S. Ryu, D. J. Kim, H. Lee, M. Y. Zhuravlev, C. B. Eom, E. Y. Tsymbal, A. Sinitskii, and A. Gruverman, Nat. Commun. **5**, 5518 (2014).

[39] B. B. Tian, J. L. Wang, S. Fusil, Y. Liu, X. L. Zhao, S. Sun, H. Shen, T. Lin, J. L. Sun, C. G. Duan, M. Bibes, A. Barthelemy, B. Dkhil, V. Garcia, X. J. Meng, and J. H. Chu, Nat. Commun. **7**, 11502 (2016).

[40] J. Müller, T. S. Böscke, D. Bräuhaus, U. Schröder, U. Böttger, J. Sundqvist, P. Kücher, T. Mikolajick, and L. Frey, Appl. Phys. Lett. **99**, 112901 (2011).

[41] J. J. Yang, D. B. Strukov, and D. R. Stewart, Nat. Nanotechnol. **8**, 13 (2013).

[42] V. K. Sangwan and M. C. Hersam, Nat. Nanotechnol. **15**, 517 (2020).

[43] V. Rouco, R. E. Hage, A. Sander, J. Grandal, K. Seurre, X. Palermo, J. Briatico, S. Collin, J. Trastoy, K. Bouzehouane *et al.*, Nat. Commun. **11**, 658 (2020).